LAYERED MATERIALS

Order-to-disorder transition due to entropy in layered and 2D carbides

Brian C. Wyatt[1], Yinan Yang[2], Paweł P. Michałowski[3]*, Tetiana Parker[4], Yamilée Morency[5], Francesca Urban[4], Givi Kadagishvili[6], Manushree Tanwar[6], Sixbert P. Muhoza[7], Srinivasa Kartik Nemani[8]†, Annabelle Bedford[1], Hui Fang[6], Zachary D. Hood[7], Junwoo Jang[8], Krutarth Kamath[1], Bethany G. Wright[8], Rebecca Disko[8], Anupma Thakur[1], Sanguk Han[5], Neil Ghosh[8], Xianfan Xu[8], Zahra Fakhraai[6]*, Yury Gogotsi[4]*, Aleksandra Vojvodic[5]*, De-en Jiang[2]*, Babak Anasori[1,8]*

In compositionally complex materials, there is controversy on the effect of enthalpy versus entropy on the structure and short-range ordering in so-called high-entropy materials. To help address this controversy, we synthesized and probed 40 M_4AlC_3 layered carbide phases containing two to nine metals and found that short-range ordering from enthalpy was present until the entropy increased enough to achieve complete disordering of the transition metals in their atomic planes. We transformed all of these layered carbide phases into two-dimensional (2D) sheets and showed the effects of the order versus disorder on their surface properties and electronic behavior. This study suggests the key effect that the competition between enthalpy and entropy has on short-range order in multicompositional materials.

Alloys containing stoichiometric mixtures of metallic elements in high-entropy alloys were systematically explored in the early 2000s (*1*, *2*). These studies demonstrated increased mechanical properties (*3*) and decreased thermal conductivity (*4*) beyond normal expectations of the "rule of mixture" approximations (*3*–*7*). In one of the early studies (*1*), it was proposed that increasing the total number of metallic elements in a single-phase material could result in entropy stabilization of enthalpically unfavorable mixtures of elements, which gained this class of metals the descriptor "high-entropy" alloys. Since this early report, high-entropy materials have been reported in other metallic alloys (*8*), as well as carbides (*9*), oxides (*10*), diborides (*11*), and other ceramics (*12*). However, since the "high-entropy" descriptor became popular, there has been push-back to using it as a general label (*13*) because it may not fully represent the major effect that enthalpy still has on the stability of a single-phase system. For example, short-range ordering in some high-entropy systems (*14*–*17*) suggests that enthalpic effects must still be present, even in entropy-stabilized materials (*18*). Therefore, there is a basic need to evaluate the true role of entropy versus enthalpy in the achieved configurations in single-phase "high-entropy" materials.

[1]School of Materials Engineering, Purdue University, West Lafayette, IN, USA. [2]Department of Chemical and Biomolecular Engineering, Vanderbilt University, Nashville, TN, USA. [3]Łukasiewicz Research Network - Institute of Microelectronics and Photonics, Warsaw, Poland. [4]A.J. Drexel Nanomaterials Institute and Department of Materials Science and Engineering, Drexel University, Philadelphia, PA, USA. [5]Department of Chemical and Biomolecular Engineering, University of Pennsylvania, Philadelphia, PA, USA. [6]Department of Chemistry, University of Pennsylvania, Philadelphia, PA, USA. [7]Applied Materials Division, Argonne National Laboratory, Lemont, IL, USA. [8]School of Mechanical Engineering, Purdue University, West Lafayette, IN, USA. ***Corresponding author. Email: banasori@purdue.edu (B.A.); de-en.jiang@vanderbilt.edu (D.J.), alevoj@seas.upenn.edu (A.V.); gogotsi@drexel.edu (Y.G.); fakhraai@sas.upenn.edu (Z.F.); pawel.michalowski@imif.lukasiewicz.gov.pl (P.P.M.)** †Present address: Department of Mechanical and Materials Engineering, University of Alabama Birmingham, Birmingham, AL, USA.

MAX phases are chemically denoted by their formula $M_{n+1}AX_n$, where M refers to n+1 layers of one or more early transition metals that are interleaved by X, which represents n layers of carbon or nitrogen (*19*). Between these $M_{n+1}X_n$ slabs, there are monoatomic layers of one or more A elements (commonly from groups 13 to 16 of the periodic table) (*20*). M is ionically or covalently bonded to X (*21*), similar to a transition metal carbide (*22*), whereas the surface M of each $M_{n+1}X_n$ slab is metallically bonded to the A element (*21*), which is structurally similar to a stacking fault in layered ceramics (*23*, *24*). As a result of this different structure and bonding at the $M_{n+1}X_n$-A-$M_{n+1}X_n$ interface, there can be a preference for the ordering of two or more transition metals in separate transition metal planes (*25*). When $n > 1$ in $M_{n+1}AX_n$, some transition metals prefer M sites bonded to both X and to A (M′ layers) or M sites only bonded to X (M″ layers), which is referred to as o-MAX (see Fig. 1A for M = 2) (*26*–*28*).

Although these o-MAX phases were reported a decade ago in two transition metal systems (*29*), the preference for an M' versus an M″ site in MAX phases is still not fully understood. Computationally, it has been shown that group 6 transition metals such as Cr, Mo, and W prefer M′ sites, whereas group 4 transition metals such as Ti, Zr, and Hf prefer M″ sites (*30*, *31*). Similarly, the earliest reported (in 2021) "high-entropy" 2D MXenes, $(TiVCrMo)_4C_3$ and $(TiVNbMo)_4C_3$ (*32*), were still predicted to have Cr and Mo in M' sites and Ti and Nb in M″ sites (*33*). Because MXenes are derived from their precursor MAX phases (*34*), this suggests that even in entropy-stabilized MAX phases (*32*), the enthalpic preference of M′ or M″ site occupancy is likely present.

We report the synthesis of 40 compositionally complex MAX phases containing two to nine transition metals. We demonstrate that MAX and MXenes let us evaluate the short-range ordering in multielemental materials and demonstrate the effects of enthalpy versus entropy on the order-to-disorder transition at the smallest scale (i.e., a few layers of atoms).

Theoretical studies of the order-to-disorder transition

To gain insight into the competition between enthalpy and entropy toward the order-disorder transition in high-entropy MAX phases (Fig. 1A), we first used density functional theory (DFT). To understand the M′ versus M″ preference for different transition metals in the M_4AlC_3 MAX phase, we built a symmetric model considering a pair of transition metals (M_1 and M_2) in either M' or M″ layers (M_1-C-M_2-C-M_2-C-M_1) for all possible combinations (from two to nine elements) (fig. S1). Figure S2 shows the formation energy (E_f) of these configurations; the calculation details are reported in the supporting information (see the materials and methods and tables S1 to S3).

After calculating these formation energies, we next used the difference in the formation energy (ΔE_f) between these structures with two given transition metals in either M′ or M″ sites to observe the enthalpic preference of the transition metals for different layers in the M_4C_3 structure (Fig. 1B). We focused on identifying the preference for out-of-plane ordering for M (i.e., to occupy separate transition metal planes), which we found to have a higher effect on the formation energy than any in-plane order (figs. S3 to S5). Trendwise, we observed that the M′ preference was Cr > Mo > W > V > Nb > Ta > Ti > Zr > Hf (inverse for M″ preference). This trend agrees with previous studies on both binary and high-entropy MAX phase (and carbide) literature showing that group 6 transition metals are usually less stable in the M_6C octahedra and, in MAX, tend to segregate toward M sites closest to the A layer (*9*, *30*). Overall, we show here that this preference is still present in M_4AlC_3 structures with more than two transition metals.

We used our model for short-range order to evaluate this hypothesis given the clear preference for transition metal arrangement in the M_4AlC_3 MAX phase structure. We first analyzed three M_4AlC_3 MAX phase structures with four transition metals: $(TiVNbTa)_4AlC_3$, $(TiVNbW)_4AlC_3$, and $(TiCrMoW)_4AlC_3$. Broadly, we found that when the same preference for order as found in double transition metal

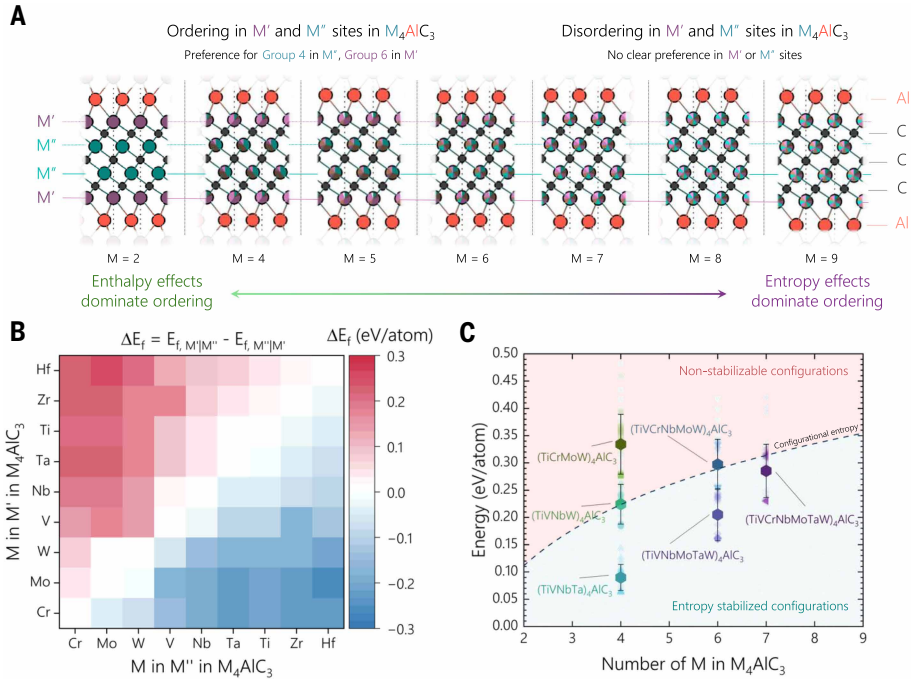

Fig. 1. Enthalpy versus entropy competition toward order-disorder in M_4AlC_3 MAX phases. (**A**) Schematic showing the hypothesis of increasing disorder with increasing entropy in M_4AlC_3 MAX phases. (**B**) Difference in formation energies for different pairs of transition metals in either M′ or M″ sites in M_4AlC_3 MAX. (**C**) Formation energy above the hull (ΔE_{hull}) versus configurational entropy in M_4AlC_3 MAX phases with the formation energy versus entropy-crossover around seven transition metals. Error bars represent SD.

o-MAX (labeled "ordered") was matched (figs. S4 to S6), the lowest formation energies were achieved. For example, when V and W occupied only M′ (outer) sites and Ti and Nb occupied only M″ (inner) sites in $(TiVNbW)_4AlC_3$, the formation energy was −0.544 ± 0.001 eV/atom. By contrast, if Ti and Nb occupied only M′ sites and V and W occupied only M″ sites, the opposite of the previous reports of o-MAX phases (labeled "inverse ordered"), then the formation energy was −0.430 ± 0.001 eV/atom. Similarly, solid-solution occupancies of Ti and Nb in M′ and M″ sites had a higher formation energy of −0.485 ± 0.006 eV/atom for $(TiVNbW)_4AlC_3$ than the ordered configuration.

Additionally, we found that group 6 elements always increased the distribution of the energy penalty because it is energetically preferred for group 6 elements to be in the M′ over the M″ sites (fig. S6). Broadly, this suggests two things: (i) MAX phases containing group 6 elements are generally less energetically favored and (ii) group 6 elements, if present, will most likely be in the M′ site. However, we found that the formation energy of MAX phases containing group 6 elements decreased with the increasing number of transition metals, which provides an avenue to their inclusion in MAX and potential MXenes (fig. S6). Therefore, after analyzing the contributions of enthalpy and entropy across several compositions (figs. S5 and S6), we predict that the transition from order to disorder likely occurs when a seventh element is introduced. However, because of the extensive computational demand, it was not feasible in the present study to simulate all possible compositions. A summary of this analysis of formation energy versus configurational entropy for the MAX phases containing four, six, and seven transition metals is shown in Fig. 1C, where the configurations below the dotted line are stabilizable by entropy and the configurations above the dotted line are not.

Experimental observation of the order-to-disorder transition due to entropy

With the gained knowledge from the energetic perspective, we next experimentally synthesized M_4AlC_3 MAX phases containing combinations of two and four to nine elements of group 4, 5, and 6 transition metals (Fig. 2, A and B). Synthesis and other details for these phases are provided in the supporting information. To determine whether we could experimentally observe ordering in M_4AlC_3 MAX phases, we first analyzed the x-ray diffraction (XRD) patterns (figs. S7 and S8). All of the 40 phases reported in this work can be found in table S4. All MAX phase characterization and analysis for each phase reported can be found in figs. S9 to S44. Figure 2C shows the scanning electron microscopy (SEM) image of $(TiVCrZrNbMoHfTaW)_4AlC_3$ with a layered grain structure; the energy-dispersive x-ray spectroscopy (EDS) shows that the grain contains all nine transition metals as well as Al (Fig. 2D). The XRD data (figs. S9 to S44) show the presence of impurity phases, including intermetallics and non-MAX carbides, which suggests that subsequent studies are required to improve the phase purity of these MAX phases. Although the XRD data provide some insight into the ordering, it is difficult to accurately compare transition metals with very similar x-ray scattering features (i.e., Ti versus V or Cr, Zr versus Nb or Mo, or Hf versus Ta or W) even when using Rietveld refinement. Therefore, we used an atomic-layer resolved dynamic secondary ion mass spectrometry (SIMS) method because this technique is better suited to differentiating the transition metals by elemental mass and charge (*35*–*37*).

To calculate the preference for site occupancy using SIMS, we determined atomic composition from the signal intensity (*37*) and calculated the average and SD of the occupancy of each element in either the M′ or M″ site. We then calculated a unitless comparative parameter, labeled α, for each transition metal from these values using Eq. 1 (*33*). As a result, when α is positive, it represents that a given transition metal prefers the M′ site. The inverse is also true. All SDs from the atomic composition were then propagated to this α using the root mean square method.

$$\alpha = \frac{M' - M''}{M' + M''} \quad (1)$$

SIMS indicates that Mo always occupies the M′ site and Ti, V, and Nb always occupy the M″ site for M_4AlC_3 MAX phases with two transition metals (fig. S45). This agrees with Fig. 1B, which states that group 6 transition metals most likely occupy M′ sites, whereas group 4 or 5 occupy M″ sites. Further, to calculate this site preference for M_4AlC_3 MAX phases with four or more transition metals, the difference in the atomic composition of each element in the M′ and M″ sites was evaluated by the α parameter (Eq. 1). Using this parameter, we noted that when four transition metals were placed into the M_4AlC_3 MAX phase, the trend in preference of a transition metal for an M′ or M″ site was the same as established for M_4AlC_3 MAX with two transition metals (Cr > Mo > W > V > Nb > Ta > Ti > Zr > Hf in M′ site) (Fig. 2E). This agrees with Fig. 1, B and C, suggesting that an enthalpic preference for M′ or M″ site ordering of the transition metals is still present even for these entropy-stabilized M_4AlC_3 MAX phases (*32*).

We observed that increasing the number of transition metals to five or six resulted in a diminished |α| for each transition metal (Fig. 2F). Together with Fig. 1C, this suggests that configurations with less preference for order are more likely to be stabilized by the increasing configurational entropy. For the SIMS data, this would result in a lower

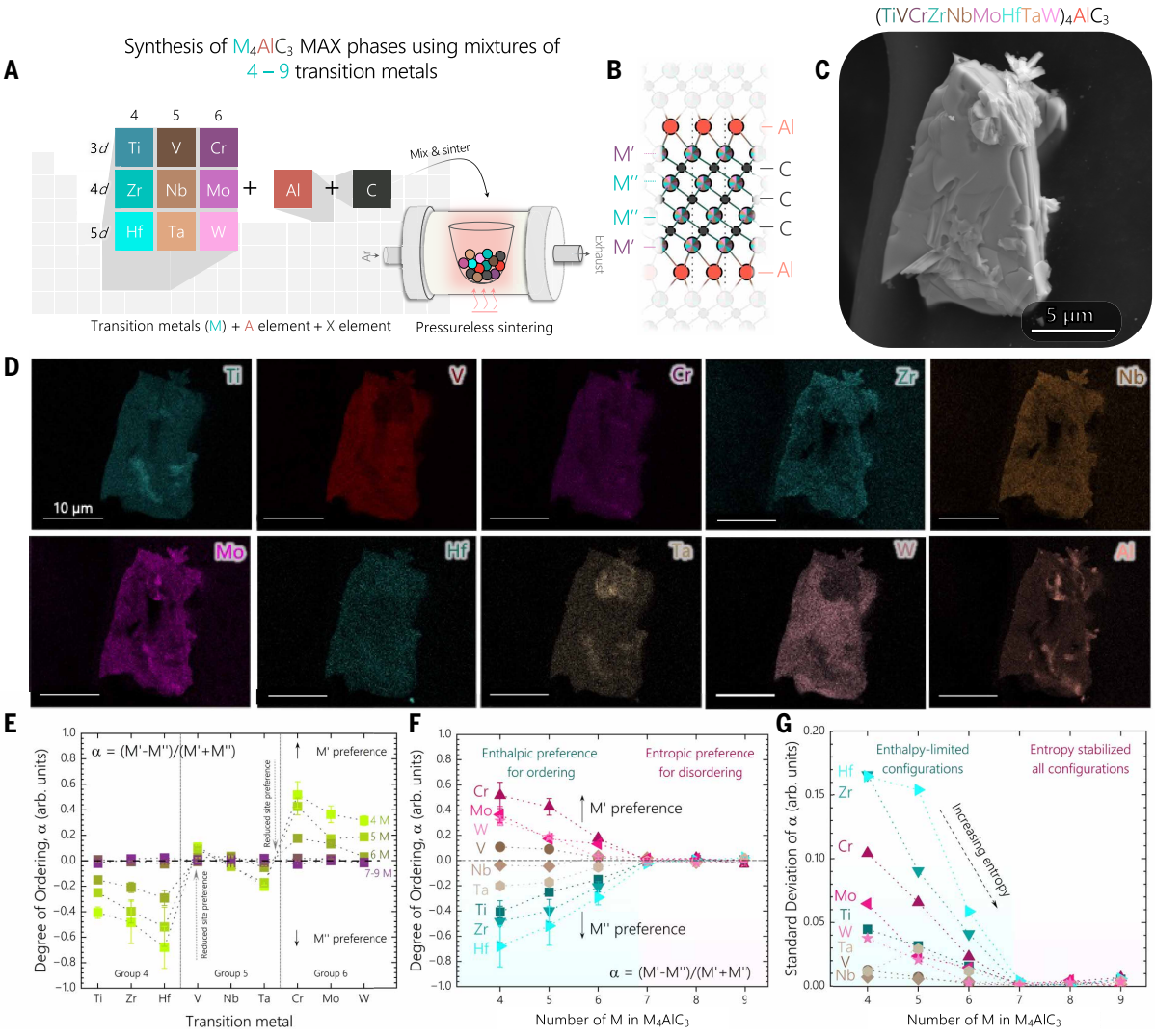

Fig. 2. Synthesis and analysis of $(TiVCrZrNbMoHfTaW)_4AlC_3$ and other M_4AlC_3 phases containing two to nine transition metals. (**A**) Schematic highlighting the mixed elements and synthesis approach. (**B**) Crystal structure of the targeted M_4AlC_3 MAX phase. (**C**) Electron microscopy image of a grain of $(TiVCrZrNbMoHfTaW)_4AlC_3$ MAX. (**D**) Elemental mapping of a grain of $(TiVCrZrNbMoHfTaW)_4AlC_3$ MAX showing the presence of all nine transition metals and aluminum. (**E**) SIMS measurements showing the preference for sites based on the transition metal and the total number of transition metals in M_4AlC_3 MAX. (**F**) SIMS showing the decreasing preference for different sites in M_4AlC_3 MAX plotted against the increasing numbers of transition metals. (**G**) Decrease in SD in the ordering term α as calculated by SIMS plotted against the increasing numbers of transition metals. Error bars represent SD.

|α| for each transition metal, because ordered (Fig. 1B) and disordered configurations of the transition metals would become observable in each transition metal layer. Probabilistically, however, we would not expect |α| to converge on zero yet in these low-to-medium–entropy systems because inverse-ordered configurations would not yet become stabilizable through entropy.

Conversely, beyond seven transition metals, we observed that the |α| converged on 0 for all transition metals (Fig. 2F). The convergence of |α| to zero suggests that ordered, solid-solution, and inverse-ordered configurations are stabilized. This would likely result in equal probabilistic chances to observe any configuration through SIMS measurements. We observed further support for this hypothesis by plotting the SD of |α| for all transition metals against the total number of transition metals (Fig. 2F), which further suggested that all configurations become stabilized at seven transition metals. Overall, our computational and experimental results indicate that the loss of short-range ordering in high-entropy MAX phases is only achievable once entropy can overcome the enthalpic penalties for all configurations. Broadly, these data demonstrate that (i) entropy-stabilized systems can display a preference for short-range ordering but (ii) systems only truly become "high-entropy" materials once entropy overcomes any remaining enthalpic preferences for the short-range order. However, high-throughput methods should be implemented to screen the effects of electronegativity, atomic size, electronic structure, oxygen substitution in the X sublattice, and other key features of the ordering and order-to-disorder transition to fully understand this transition. Further, subsequent studies must consider the impact of intermediate phases on the final phase formation and ordering. Although computational studies have shown that out-of-plane ordering trends are similar between $M_{n+1}AX_n$ phases with $n > 2$, subsequent studies should evaluate whether order-to-disorder transitions would be observed in other multitransition metal MAX phases.

Effect of order versus disorder on MXene surface chemistry

After confirming the synthesis and ordering behavior of the M_4C_3 structure in the M_4AlC_3 MAX phases, we evaluated the effect of order versus disorder and composition on the individual M_4C_3 lamellas. To do so, we synthesized the $M_4C_3T_x$ MXenes from their M_4AlC_3 MAX

phases using wet chemical synthesis (Fig. 3A) (*28*, *31*, *32*, *34*), which causes the MXene surface to be terminated with T groups, commonly –O, –OH, and –F (*34*). Some XRD patterns of MAX to MXene synthesis are shown in fig. S46. Further, we confirmed that our MXenes contained the same transition metals as the MAX, as shown for $(TiVCrZrNbMoHfTaW)_4C_3T_x$ in figs. S47 and S48. In addition, we used SIMS to confirm that the ordering of the transition metals remained similar in the MXenes as it was in the MAX for some select compositions (figs. S49 to S52). We were also able to successfully synthesize MXene films for a total number of transition metals between four and nine, as shown through XRD in fig. S53. Although we used a similar etching procedure for all MAX phases to obtain MXenes, subsequent studies are necessary to understand the exfoliation energy of each MAX to MXenes to best tune the synthesis process for any individual composition (*38*). All 2D MXenes produced in this study were dispersible in water (fig. S54). However, using x-ray photoelectron spectroscopy (XPS), we observed that the overall composition of T_x in the $M_4C_3T_x$ MXenes containing four to nine transition metals increased for –O (~33 at % to ~53 at %) and decreased for –OH (~37 at % to ~26 at %) and –F (~30 at % to 21 at %) (figs. S55 to S63 and table S5).

The ordering or disordering observed in the MAX phases is present in the MXenes (*36*) (figs. S49 to S52) and is a likely source of the changes in the T_x group composition in the respective $M_4C_3T_x$ MXenes. To gain insight into this trend, we used DFT to calculate the formation energy of –O and –F terminations on MXenes with different pairs of transition metals in either M′ or M″ sites (Fig. 3B). We observed that pairs of group 4 elements preferred F terminations, and pairs of group 6 elements preferred O terminations. We also observed that group 6 in M″ sites caused an increased preference for group 4 in M′ for O terminations, and group 4 in M″ sites caused an increased preference for group 6 in M′ for F terminations. As shown in the supporting information (fig. S64), the solid-solution combinations were typically between the two ordered configurations. The calculated values of O versus F preference for both ordered and solid-solution configurations of the paired transition metals are shown in fig. S65.

Because we cannot know the exact subsurface M″ metal atom for any given M′ metal atom bonded to T_x in our MXenes, we chose to plot the surface chemistry for M in M′ sites (bonded to T_x) against the valence electron concentration (VEC) in the M″ sites (Fig. 3, C and D), which was derived from SIMS using formal charges of the transition metals (Ti has four, V has five, Cr has six, etc.). In addition, in this plot, we consider both –OH and –F terminations together and –O terminations separately because –OH and –F would prefer a T^- oxidation state, whereas –O would prefer a T^{2-} oxidation state. In addition, we chose to add –OH and –F together because our use of tetramethylammonium hydroxide as a delamination agent could replace –F groups with –OH groups, and the two share a formal charge. As shown in Fig. 3, C and D, increasing the VEC in the M″ sites can increase the concentration of O terminations on Ti and –OH/F on V and Mo, which is broadly in agreement with the trends shown in Fig. 3B. A plot for easier comparison can be found in fig. S66. We observed agreement with the general increase of O as a T_x group on $M_4C_3T_x$ MXenes containing four to nine transition metals (see Fourier transform infrared spectra in fig. S67). In addition, through ultraviolet–visible–near infrared and Raman spectroscopy, we gained some insight into the effect of disorder in $M_4C_3T_x$ MXenes by increasing the total number of transition metals (figs. S68 to S71). Overall, this suggested that surface versus subsurface transition metals affect the chemical behavior and preference for surface terminations of the MXenes (*39*).

Effect of order versus disorder on MXene electrical conductivity

We evaluated the effect of multiple transition metals and order versus disorder on the electrical properties of thin films of these $M_4C_3T_x$ MXenes. When we investigated the $M_4C_3T_x$ MXenes containing two to nine transition metals, we found that the MXenes retained their metallic conductivity, as shown by both their linear *I* versus *V* behavior and their consistency with the Drude model of metallic electrical conductivity (figs. S72 to S78) (*40*). In addition, we noted that MXenes that contained Cr were up to an order of magnitude higher in electrical resistivity (fig. S79), which has been reported for high-entropy alloys

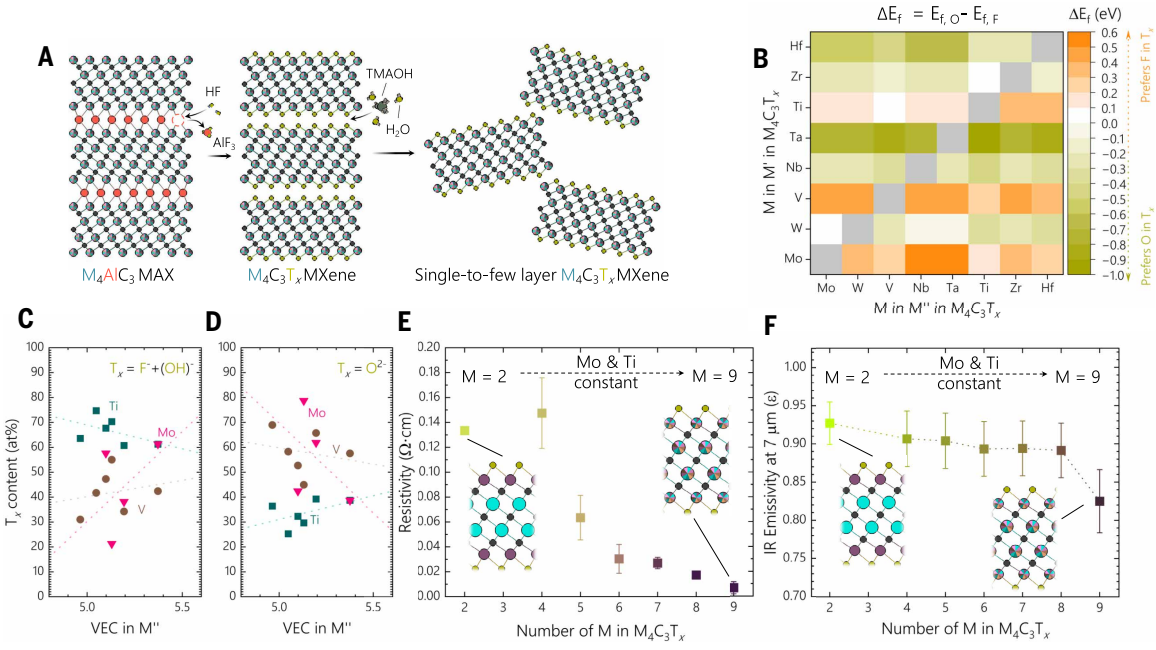

Fig. 3. Synthesis, surface chemistry, and properties of $M_4C_3T_x$ MXenes containing two to nine transition metals. (**A**) Schematic of the synthesis process of $M_4C_3T_x$ MXenes from M_4AlC_3 MAX. (**B**) Differences in formation energy of pairs of transition metals in $M_4C_3T_x$ with O versus F in termination sites (T). The gray boxes represent values for single-metal MXenes, which were not calculated in this study. (**C** and **D**) Content of O and F terminations, respectively, on Ti, V, and Mo atoms in $M_4C_3T_x$ MXenes versus the VEC in the M″ layers. The dotted lines are guides for the eye. (**E**) Electrical resistivity behavior of $M_4C_3T_x$ MXenes containing two to nine transition metals. (**F**) IR emissivity at 7-μm wavelength plotted against the total number of transition metals in the $M_4C_3T_x$ MXenes. Error bars represent experimental uncertainty.

with Cr (*41*). The flake sizes are shown using dynamic light scattering measurements in fig. S80. In figs. S81 to S89, atomic force microscopy images, height, and surface roughness analysis of some of the $M_4C_3T_x$ flakes containing two to nine transition metals are shown (table S6 summarizes the height and surface roughness results).

Decreasing electrical resistivity has been reported for high-entropy alloys with increasing numbers of transition metals (*42*), but the cause for this is not yet fully understood. In M_2C-type MXenes, computational work has shown that group 5 transition metals in MXenes should lower the electrical resistivity (*43*), whereas group 6 transition metals in MXenes have a higher electrical resistivity (*44*). Overall, in our high-entropy $M_4C_3T_x$ MXenes, we expected an increasing number of transition metals to cause disorder of group 5 and 6 transition metals throughout the $M_4C_3T_x$ structure. Therefore, we first plotted the electrical resistivity of our $M_4C_3T_x$ MXenes against the total number of transition metals, as shown in Fig. 3E. In Fig. 3E, we chose to keep Ti and Mo as consistent transition metals and systematically add one transition metal at a time to maintain comparability between samples. For example, at M = 2, we showed the fully ordered $Mo_2Ti_2C_3T_x$, and at M = 4, we showed the low entropy $(TiVNbMo)_4C_3T_x$ and then added W, Ta, Cr, Zr, and Hf for M = 5, 6, 7, 8, and 9, respectively.

In Fig. 3E, it can be seen that the resistivity of $Mo_2Ti_2C_3T_x$ at 0.13 Ω×cm initially increased for $(TiVNbMo)_4C_3T_x$ to 0.15 ± 0.03 Ω×cm and then decreased to 0.01 ± 0.01 Ω×cm $(TiVCrZrNbMoHfTaW)_4C_3T_x$. In addition, we observed a similar behavior in the infrared (IR) emissivity of these MXenes (Fig. 3F). This agrees with the changes in electrical resistivity shown in Fig. 3E, because decreasing electrical resistivity typically will result in a proportional decrease in IR emissivity (*45*). Broadly, we hypothesize that this decrease in resistivity could be attributed to two things (fig. S90): (i) the decrease in ordering results in fewer neighbors of group 6 to group 6 transition metals and (ii) the decrease in order creates structures with smaller differences in the total number of valence electrons (averaging to five) between neighbors in both M′ and M″ layers, both of which could improve the electron mobility in and between the M′ and M″ layers. However, subsequent studies are necessary to better understand the electron mobility and other properties in high-entropy MXenes and other high-entropy materials (*46*), such as approaches that focus on single-flake measurements or optical conductivity (fig. S91).

In summary, this work demonstrates a broad advancement in our understanding of the relation of enthalpy and entropy on short-range ordering in high-entropy materials. Specifically, by using M_4AlC_3 MAX phases with two to nine transition metals and analyzing their structural ordering using SIMS, we were able to evaluate the trend in the short-range ordering of transition metals in either outer (M′) or inner (M″) metal sites against the total number of transition metals. Doing so, we have shown that (i) in low- and medium-entropy combinations (i.e., up to six metals), the transition metals enthalpically prefer order in M′ or M″ sites; (ii) at seven metals or above, the structures become fully disordered (i.e., no clear preference for M′ or M″); and (iii) that this order-disorder transition is driven by an increasing contribution of configurational entropy. Finally, we showed that these MAX phases can be used to synthesize their respective MXenes, which allowed us to observe some effects of entropically driven disorder in these phases on the electrical and IR emissivity properties of these derived MXenes.

REFERENCES AND NOTES

1. J. W. Yeh *et al.*, *Adv. Eng. Mater.* **6**, 299–303 (2004).
2. B. Cantor, I. Chang, P. Knight, A. Vincent, *Mater. Sci. Eng. A* **375-377**, 213–218 (2004).
3. D. Utt *et al.*, *Nat. Commun.* **13**, 4777 (2022).
4. H.-P. Chou, Y.-S. Chang, S.-K. Chen, J.-W. Yeh, *Mater. Sci. Eng. B* **163**, 184–189 (2009).
5. L. Han *et al.*, *Nat. Rev. Mater.* **9**, 846–865 (2024).
6. S. Schweidler *et al.*, *Nat. Rev. Mater.* **9**, 266–281 (2024).
7. Y. Zhang, T. Zuo, Y. Cheng, P. K. Liaw, *Sci. Rep.* **3**, 1455 (2013).
8. F. Otto, Y. Yang, H. Bei, E. P. George, *Acta Mater.* **61**, 2628–2638 (2013).
9. P. Sarker *et al.*, *Nat. Commun.* **9**, 4980 (2018).
10. C. M. Rost *et al.*, *Nat. Commun.* **6**, 8485 (2015).
11. J. Gild *et al.*, *Sci. Rep.* **6**, 37946 (2016).
12. C. Oses, C. Toher, S. Curtarolo, *Nat. Rev. Mater.* **5**, 295–309 (2020).
13. M. Brahlek *et al.*, *APL Mater.* **10**, 110902 (2022).
14. S. Chen *et al.*, *Nat. Commun.* **12**, 4953 (2021).
15. P. Singh, A. V. Smirnov, D. D. Johnson, *Phys. Rev. B* **91**, 224204 (2015).
16. A. J. Wright, J. Luo, *J. Mater. Sci.* **55**, 9812–9827 (2020).
17. B. Jiang *et al.*, *J. Am. Chem. Soc.* **143**, 4193–4204 (2021).
18. S. Divilov *et al.*, *Nature* **625**, 66–73 (2024).
19. M. Dahlqvist, M. W. Barsoum, J. Rosen, *Mater. Today* **72**, 1–24 (2024).
20. M. Sokol, V. Natu, S. Kota, M. W. Barsoum, *Trends Chem.* **1**, 210–223 (2019).
21. M. Magnuson, M. Mattesini, *Thin Solid Films* **621**, 108–130 (2017).
22. B. C. Wyatt, S. K. Nemani, G. E. Hilmas, E. J. Opila, B. Anasori, *Nat. Rev. Mater.* **9**, 773–789 (2024).
23. A. Gusev, A. Kurlov, V. Lipatnikov, *J. Solid State Chem.* **180**, 3234–3246 (2007).
24. C. R. Weinberger, G. B. Thompson, *J. Am. Ceram. Soc.* **101**, 4401–4424 (2018).
25. M. Dahlqvist, J. Rosen, *Nanoscale* **14**, 10958–10971 (2022).
26. W. Hong, B. C. Wyatt, S. K. Nemani, B. Anasori, *MRS Bull.* **45**, 850–861 (2020).
27. B. Anasori *et al.*, *J. Appl. Phys.* **118**, 094304 (2015).
28. B. C. Wyatt *et al.*, *Nano Lett.* **23**, 931–938 (2023).
29. Z. Liu *et al.*, *J. Am. Ceram. Soc.* **97**, 67–69 (2014).
30. M. Dahlqvist, J. Rosen, *Nanoscale* **12**, 785–794 (2020).
31. B. Anasori *et al.*, *ACS Nano* **9**, 9507–9516 (2015).
32. S. K. Nemani *et al.*, *ACS Nano* **15**, 12815–12825 (2021).
33. Z. Leong *et al.*, *Chem. Mater.* **34**, 9062–9071 (2022).
34. K. R. G. Lim *et al.*, *Nat. Synth.* **1**, 601–614 (2022).
35. P. P. Michałowski *et al.*, *Nat. Nanotechnol.* **17**, 1192–1197 (2022).
36. B. C. Wyatt *et al.*, *Nat. Commun.* **15**, 6353 (2024).
37. P. P. Michałowski, *Nanoscale Horiz.* **9**, 1493–1497 (2024).
38. R. Khalediali dusti, M. Khazaei, S. Khazaei, K. Ohno, *Nanoscale* **13**, 7294–7307 (2021).
39. Y. Yang *et al.*, *2D Materials* **7**, 025015 (2020).
40. M. Han *et al.*, *ACS Nano* **14**, 5008–5016 (2020).
41. K. Jin *et al.*, *Sci. Rep.* **6**, 20159 (2016).
42. S. K. Dewangan, C. Nagarjuna, V. Kumar, in *High Entropy Materials*, A. Kumar, R. K. Gupta, Eds. (CRC Press, 2024), pp. 91–106.
43. M. Han *et al.*, *J. Am. Chem. Soc.* **142**, 19110–19118 (2020).
44. M. Khazaei, M. Arai, T. Sasaki, M. Estili, Y. Sakka, *Phys. Chem. Chem. Phys.* **16**, 7841–7849 (2014).
45. M. Han *et al.*, *Mater. Today* **64**, 31–39 (2023).
46. J.-W. Yeh, *Eur. J. Control* **31**, 633–648 (2006).

ACKNOWLEDGMENTS

G.K. and Z.F. thank T. E. Mallouk of the University of Pennsylvania for giving us access to the UV-Vis-NIR spectrometer and the Harrick Plasma Cleaner and R. Stephens for providing valuable ideas. **Funding:** This work was supported by the National Science Foundation (Center for Chemical Innovation M-STAR program grant CHE-2318105 to B.C.W., Y.Y., T.P., Y.M., F.U., G.K., M.T., S.K.N., A.B., H.F., K.K., B.G.W., R.D., A.T., S.H., Z.F., Y.G., A.V., D.J., and B.A.; Solid State & Materials Chemistry program grant DMR-2419026 to B.C.W., S.K.N., A.B., K.K., B.G.W., R.D., A.T., and B.A.; grant CBET-2051525 to J.J., N.G., and X.X.); National Science Centre, Poland (SONATA BIS 14 2024/54/E/ST11/00171 to P.P.M.); National Centre for Research and Development, Poland (LIDER XII LIDER/8/0055/L-12/20/NCBR/2021 to P.P.M.); Laboratory Directed Research and Development (LDRD) of Argonne National Laboratory, Office of Science, US Department of Energy (contract DE-AC02-06CH11357 to S.P.M. and Z.D.H.); the Vagelos Institute for Energy Science and Technology, University of Pennsylvania (graduate fellowship to Y.M.); the National Energy Research Scientific Computing Center, a DOE Office of Science User Facility (supported by the Office of Science of the US Department of Energy contract DE-AC02-05CH11231 using NERSC award BES-ERCAP0023161 to Y.M. and A.V.); and the Ministry of Trade, Industry, and Energy (MOTIE) Korea (Global Industrial Technology Cooperation Center program grant P0028332 supervised by the Korea Institute for Advancement of Technology to B.C.W., Y.G., and B.A.). **Author contributions:** Conceptualization: B.C.W., B.A. Investigation: B.C.W., Y.Y., P.P.M., T.P., Y.M., F.U., G.K., M.T., S.P.M., S.K.N., A.B., H.F., J.J., K.K., B.G.W., R.D., A.T., S.H., N.G., X.X. Methodology: B.C.W., P.P.M., S.K.N., Y.G., A.V., D.J., B.A. Project administration: B.C.W., Z.F., Y.G., A.V., D.J., B.A. Supervision: X.X., Z.F., Y.G., A.V., D.J., B.A. Writing – original draft: B.C.W., Y.Y., T.P., G.K., S.K.N., J.J., K.K. Writing – review & editing: All authors. **Competing interests:** B.C.W. and B.A. declare that a provisional patent on the synthesis of high-entropy MAX phases has been filed under patent number 70880-01. Y.G. declares his role as a board member of MXene Inc. and is also affiliated with Sumy State University, Ukraine. The remaining authors declare no competing interests. **Data availability:** All data are available in the main manuscript or the supplementary materials.

SUPPLEMENTARY MATERIALS

science.org/doi/10.1126/science.adv4415
Materials and Methods; Supplementary Text; Figs. S1 to S91; Tables S1 to S6; References (*47*–*68*)

Submitted 19 December 2024; accepted 1 July 2025

10.1126/science.adv4415